J Solid State Electrochem (2005) 9: 738–749
DOI 10.1007/s10008-005-0689-z

ORIGINAL PAPER

Jörg Maurer · Rainer F. Winter · Biprajit Sarkar
Stanislav Záliš

Electron delocalization in mixed-valence butadienediyl-bridged diruthenium complexes

Published online: 14 September 2005

Abstract We report electrochemical and spectroelectrochemical investigations on the butadienediyl-bridged diruthenium complexes $[\{Ru(PPh_3)_2(CO)Cl\}_2(\mu\text{-}C_4H_4)]$ (**1**), $[\{Ru(PEt_3)_3(CO)Cl\}_2(\mu\text{-}C_4H_4)]$ (**2**), and $[\{Ru(PPh_3)_2(CO)Cl(NC_5H_4COOEt\text{-}4)\}_2(\mu\text{-}C_4H_4)]$ (**3**). All these complexes are oxidized in two consecutive one-electron steps separated by 315 to 680 mV, depending on the co-ligands. The first oxidation is a chemically and electrochemically reversible process whereas the second varies from nearly reversible to irreversible at room temperature. We have generated and investigated the mixed-valence monocations and observed CO band shifts of ca 25 cm^{-1} and the appearance of new bands in the visible regime at ca 720 to 800 and 430 to 450 nm. The lower-energy band which tails into the near infrared has been assigned as a charge-resonance (or intervalence charge-transfer) absorption and used to estimate the electronic coupling parameter H_{AB}. Our investigations point to valence delocalization for $\mathbf{2}^+$, and nearly delocalized behavior for $\mathbf{1}^+$ and $\mathbf{3}^+$. Even the complex with the smallest potential splitting is, however, fully delocalized on the longer ESR timescale, as is evident from the coupling pattern of the solution spectrum. Overall IR band shifts on full oxidation and the hyperfine splittings for $\mathbf{1}^+$ argue for charge and spin delocalization onto the bridging C_4H_4 ligand. This issue has also been addressed by quantum chemical calculations employing DFT methods. Geometry optimizations at each oxidation level reveal inversion of the C–C bond pattern from a short–long–short to a long–short–long alteration and a bis(carbenic) structure at the dication stage. All spectroscopic features such as IR band shifts, average *g*-values and *g*-tensor anisotropies are fully reproduced by the calculations.

Keywords Electrochemistry · Spectroelectrochemistry · Ruthenium · DFT calculations

Presented at the 3rd Chianti Electrochemistry Meeting, July 3.–9.2004, Certosa di Pontignano, Italy

J. Maurer · B. Sarkar
Institut für Anorganische Chemie, Universität Stuttgart,
Pfaffenwaldring 55, 70569 Stuttgart, Germany

S. Záliš
J. Heyrovský Institute of Physical Chemistry,
Academy of Sciences of the Czech Republic,
Dolejškova 3, Prague, Czech Republic

Present address: R. F. Winter (✉)
Institut für Anorganische Chemie,
Universität Regensburg, Universitätsstraße 31,
93040 Regensburg, Germany
E-mail: rainer.winter@chemie.uni-regensburg.de
Fax: +49 941 943 4488

Introduction

Since the discovery of the Creutz–Taube ion in 1969 [1], systems with two terminal redox-active moieties bridged by a π-conjugated ligand that provides a pathway for charge and spin delocalization have excited the minds of researchers. Among the plethora of complexes that comply with this general construction principle, those with unsaturated carbon chains as bridging ligands have become especially popular. This is particularly true for shorter chain polyynediyl bridges, where the easy formation of the metal–alkynyl bond and the substantial strength of the electronic coupling conveyed by these ligands combine in a highly favorable manner. Examples are dimetal complexes of the diynediyl C_4-ligand. Their monooxidized forms typically exhibit complete valence delocalization even on the short IR timescale [2, 3, 4, 5, 6, 7, 8, 9] and are thus authentic examples of strongly coupled Class-III systems according to the Robin and Day classification scheme [10]. Similar investigations on butadienediyl (–CH=CH–CH=CH–) bridged complexes are less numerous. Nevertheless, Sponsler [11, 12, 13, 14], Lapinte [15], and their coworkers have elegantly shown that the C_4H_4 ligand couples $(\eta^5\text{-}C_5R_5)L_2Fe$ centers almost as strongly as its higher unsaturated C_4 counterpart.

In 1998 Jia and co-workers established the double hydrometallation of diacetylene by [$HRu(CO)Cl(PPh_3)_3$] as a route to butadienediyl bridged diruthenium complexes. They prepared and characterized the dinuclear [$\{Ru(PPh_3)_2(CO)Cl\}_2(\mu\text{-}C_4H_4)$] (**1**) with coordinatively unsaturated metal centers, its saturated bis-NH_3 adduct and the substitution product [$\{Ru(PEt_3)_3(CO)Cl\}_2(\mu\text{-}C_4H_4)$] (**2**) [16]. To the best of our knowledge, no electrochemical investigations have been reported on these systems. Likewise, no attempts have been made to generate and characterize their oxidized forms and to address the issue of the electronic coupling in the mixed-valence state. Here we report our results from electrochemical and spectroelectrochemical studies on [$\{Ru(PPh_3)_2(CO)Cl\}_2(\mu\text{-}C_4H_4)$] (**1**), [$\{Ru(PEt_3)_3(CO)Cl\}_2(\mu\text{-}C_4H_4)$](**2**), and [$\{Ru(PPh_3)_2(CO)Cl(NC_5H_4COOEt\text{-}4)\}_2(\mu\text{-}C_4H_4)$] (**3**), the isonicotinate adduct of **1**. The structures of compounds **1**–**3** are shown in Scheme 1.

Materials and methods

All manipulations were performed by standard Schlenk techniques under an argon atmosphere. Dichloromethane was dried by distillation from CaH_2 and methanol by distillation over Mg. All solvents were degassed by either at least three freeze–pump–thaw cycles or saturation with argon before use. [$HRu(CO)Cl(PPh_3)_3$] [17] and [$\{Ru(CO)Cl(PEt_3)_3\}_2(\mu\text{-}C_4H_4)$](**2**) [16] were obtained according to the literature and [$\{Ru(CO)Cl(PPh_3)_2\}_2(\mu\text{-}C_4H_4)$] by a slight modification of the published procedure (i.e. by using neat diacetylene instead of $Me_3SiC_4SiMe_3/NBu_4F/THF$) [16]. Butadiyne was prepared from 1,4-dichloro-2-butyne (Lancaster) on a 4-mmol scale by a slight modification of a published procedure [18] and isolated at 195 K as a white, crystalline solid.

CAUTION: Butadiyne should be handled and stored with rigorous exclusion of air and at temperatures below 230 K. It was stored at 213 K. Before use, it was thawed in an ice/$CaCl_2$ cooling bath and the required amount (ca 600 μL) was transferred via a precooled pipette.

Infrared spectra were obtained on a Perkin–Elmer Paragon 1000 PC FT-IR instrument. ^1H (250.13 MHz), ^{13}C (62.90 MHz) and ^{31}P NMR spectra (101.26 MHz) were recorded on a Bruker AC 250 spectrometer as $CDCl_3$ or CD_2Cl_2 solutions at 303 K. The spectra were referenced to the residual protonated solvent (^1H), the solvent signal itself (^{13}C), or external H_3PO_4 (^{31}P). Assignment of ^{13}C NMR spectra was aided by DEPT-135 experiments. UV–visible spectra were obtained on an Omega 10 spectrometer from Bruins Instruments in Helma quartz cuvettes with 1-cm optical path lengths. The ESR equipment comprised a Bruker ESP 3000 spectrometer equipped with an HP 5350 B frequency counter, a Bruker NMR ER 035 M gaussmeter, and an ESR 900 continuous flow cryostat from Oxford Instruments for low-temperature work. Elemental analysis (C, H, N) was performed in-house. All electrochemical experiments were performed in a home-built cylindrical vacuum-tight one-compartment cell. A spiral-shaped Pt wire and a Ag wire as the counter and reference electrodes are sealed directly into opposite sides of the glass wall while the respective working electrode (Pt or glassy carbon, 1.1 mm, polished with 0.25 μm diamond paste (Buehler–Wirtz) before each experiment) are introduced via a Teflon screw-cap with a suitable fitting.

The cell may be attached to a conventional Schlenk line via two side-arms equipped with Teflon screw valves and enables experiments to be performed under an atmosphere of argon with approximately 2.5 mL of analyte solution. CH_2Cl_2 and 1,2-$C_2H_4Cl_2$ for electrochemical work were obtained from Fluka (Burdick and Jackson Brand) and freshly distilled from CaH_2 before use. NBu_4PF_6 (0.25 mmol L^{-1}) was used as the supporting electrolyte. All potentials are referenced relative to the ferrocene/ferrocenium couple. Electrochemical data were acquired with a computer controlled EG&G model 273 potentiostat utilizing the EG&G 250 software package.

The optically transparent thin-layer electrolysis (OTTLE) cell was also home built following the design of Hartl et al. [19] and comprised Pt-mesh working and counter electrodes and a thin silver wire as a pseudo-reference electrode sandwiched between the CaF_2 windows of a conventional liquid IR cell. The working electrode was positioned in the center of the spectrometer beam.

Synthesis of [$\{Ru(PPh_3)_2(CO)Cl(NC_5H_4COOEt\text{-}4)\}_2(\mu\text{-}C_4H_4)$] (**3**)

To a suspension of complex **1** (0.0499 mmol, 0.06 g) in CH_2Cl_2 (10 mL) was added a solution of ethyl isonicotinate (0.015 mL, 0.0998 mmol) in CH_2Cl_2 (10 mL).The reaction mixture was stirred for 20 min at room temperature to generate complex **3**. The solvent was removed under vacuum and the red precipitate was

Scheme 1

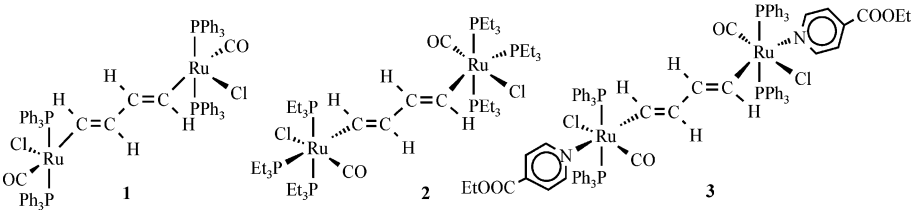

washed twice with 5 mL diethyl ether and dried under vacuum for 3 h. Yield: 0.061 g, 70%. IR (KBr, ν in cm^{-1}) 1922 (CO), 1716 (COOEt), 1480 (C=C). ^{31}P NMR (101.256 MHz, $CDCl_3$) δ 27.0 (broad s); ^{1}H NMR (250 MHz, $CDCl_3$) δ 8.59 [4H, broad s, py], 7.52–7.45 [20H, m, PPh_3], 7.29–7.00 [46H, m, py, PPh_3, C=CH (bridge)], 5.4 [2H, broad d, $^{3}J_{H\text{-}H}=11.5$ Hz, HC=C (bridge)], 4.35 [4H, q, $^{3}J_{H\text{-}H}=7.14$ Hz, CH_2 (isonicotinate)], 1.37 [6H, t, $^{3}J_{H\text{-}H}=7.14$ Hz, CH_3 (isonicotinate)]. Elemental analysis: Found: C, 65.00%; H, 4.70%, N, 1.22%, calcd: C, 65.16%; H, 4.77%; N, 1.63%.

Molecular orbital calculations

The ground-state electronic structure was calculated by density functional theory (DFT) methods using the ADF2002.3 [20, 21] and Gaussian 03 program packages [22]. Slater type orbital (STO) basis sets of triple ζ quality with polarization functions were employed with the exception of the CH_3 substituents on P atoms which were described on a double ζ basis. The inner shells were represented by a frozen core approximation, viz. 1 s for C, N, 1s-2p for P, Cl and 1s-3d for Ru were kept frozen. The following density functionals were used within ADF: a local density approximation (LDA) with VWN parametrization of electron gas data and a functional including Becke's gradient correction [23] to the local exchange expression in conjunction with Perdew's gradient correction [24] to the LDA expression (ADF/BP). The scalar relativistic (SR) zero-order regular approximation (ZORA) was used within this study. The *g*-tensor was obtained from a spin-nonpolarized wave function after incorporating the spin–orbit (SO) coupling by first-order perturbation theory from the ZORA Hamiltonian in the presence of a time-independent magnetic field [25, 26]. Within G03 calculations the quasirelativistic effective core pseudopotentials and the corresponding optimized set of basis functions for Ru [27] and 6–31G* polarized double-ζ basis sets [28] for the remaining atoms were employed together with the B3LYP [29] or BP86 [23, 24] functional. Geometry optimization and vibrational analysis were performed on the $[\{RuCl(CO)(PMe)_3\}_2(\mu\text{-}CH=CHCH=CH)]^{n+}$ ($n=0,1,2$) model systems. Open-shell systems were treated using unrestricted Kohn Sham calculations. The calculations were performed without any symmetry constraints.

Results

Electrochemistry and spectroelectrochemistry

Hydrometallation of terminal alkynes by $[HRu(CO)Cl(PPh_3)_3]$ is a highly reliable and convenient route to ruthenium vinyl complexes because it proceeds in a regio- and stereospecific manner. The metal usually becomes attached to the unsubstituted carbon atom and the former hydride ligand occupies a position *cis* to the ruthenium atom [30, 31, 32]. The use of α,ω-dialkynes for the formation of dinuclear complexes is widely reported in the literature, including diethynylarenes [33, 34], tetraethynylbiphenyls [33], diethynylalkanes [35], and diethynylalkenes [16, 36, 37]. Voltammetric investigations on the C_6H_6 and C_8H_8 bridged congeners $[\{RuCl(CO)(PMe_3)_3\}_3(\mu\text{-}(CH=CH)_n)]$ ($n=3,4$) have shown two separate one-electron oxidation events. The redox splittings of 300 and 240 mV, respectively, suggest considerable metal–metal interactions across the $-(CH=CH)_n-$ bridge. To the best of our knowledge, no such investigations have been published on the butadienediyl congeners, in which even stronger interactions are expected, because of the decreased length of the conjugated spacer [16].

Cyclic voltammetry of compounds **1–3** in CH_2Cl_2/NBu_4PF_6 solutions indicates that each complex is oxidized in two consecutive one-electron steps. The first anodic wave always constitutes a chemically and electrochemically reversible couple as judged by the usual criteria. The second oxidation is, however, only partially reversible for **1** and **3** and completely irreversible for complex **2**, indicating that the second electron transfer is followed by a fast chemical step (Fig. 1). The following reaction(s) can be partially suppressed by applying faster sweep rates or immersing the cell in a dry ice–isopropanol slush bath. For **2** this was only possible to an extent that enabled us to detect the associated counter peak and thus establish the half-wave potential of the $\mathbf{2}^{+/2+}$ couple. For this compound a third partially

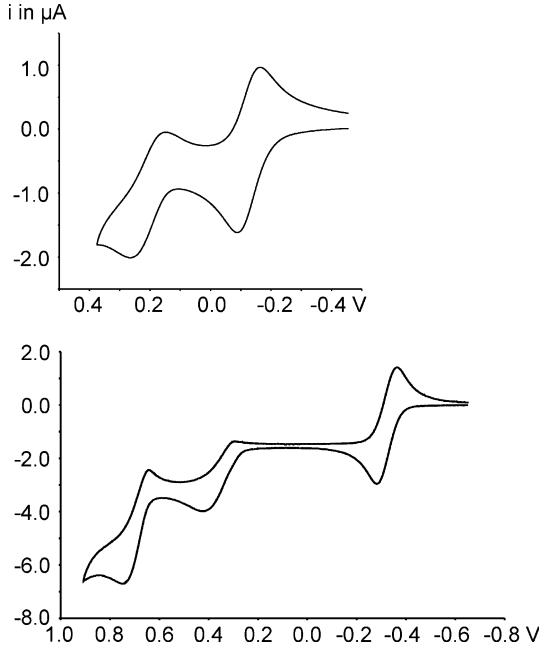

Fig. 1 Voltammetric traces for complexes **1** ($v=0.2$ V s^{-1}, 293 K, *upper trace*) and **2** ($v=0.1$ V s^{-1}, 195 K, *lower trace*) in CH_2Cl_2/NBu_4PF_6

Table 1 Electrochemical data for complexes**1–3** in CH_2Cl_2/NBu_4PF_6 (0.2 mol L^{-1}); potentials are given relative to the ferrocene/ferrocenium standard

Compound	$E_{1/2}{}^{0/+}$ in V (ΔE_p in mV)	$E_{1/2}{}^{+/2+}$ in V (ΔE_p in mV)	$\Delta E_{1/2}$ in V (K_c)[a]
1	−0.125 (60)	0.190 (75)[b]	0.315 (2.1×10^5)
2[c]	−0.325 (60)	0.355 (94)[d]	0.680 (3.2×10^{11})
3	−0.260 (120)	0.315 (132)[b]	0.575 (5.3×10^9)

[a]Comproportionation equilibrium constant as calculated by use of Eq. 2
[b]Only partially reversible wave
[c]An additional partially reversible couple at 0.495 V is observed
[d]Nearly irreversible wave

reversible anodic peak is observed. Given the irreversibility of the previous second oxidation, its assignment remains, however, unclear at this point. Relevant data from voltammetric investigations are collected in Table 1. Fig. 1 compares the voltammetric traces of compounds **1** and **2**.

The reversibility of the first oxidation processes suggests that the monooxidized forms of **1**-**3** are easily accessible. Electrochemical oxidation inside an OTTLE cell [19] with IR, UV–visible, and NIR spectroscopic monitoring cleanly converted the neutral starting compounds to their corresponding radical cations, as is indicated by isosbestic points and nearly complete reconversion to the parent neutrals on subsequent reduction. It has already been noted that thin-layer conditions may enable the detection of otherwise highly reactive species that are not so easily accessible by other means [6, 38]. This was also true in our work. Despite the only partially reversible or even irreversible nature of the second oxidation waves of complexes **1** to **3**, it was still possible to generate and spectroscopically characterize their respective dications inside the OTTLE cell. Whereas **1** and **3** exhibited good isosbestic points under these conditions, dioxidized $\mathbf{2}^{2+}$ was only observed as a transient species, but at sufficient concentrations to establish its main spectroscopic features.

When the first oxidation is performed with IR monitoring, the initial single carbonyl CO bands of the neutrals are replaced by one new absorption at approximately 25 cm^{-1} higher energy (Table 2, Fig. 2). For $\mathbf{2}^+$ the new CO band is as sharp as in the neutral starting complex whereas for $\mathbf{1}^+$ and $\mathbf{3}^+$ it is substantially broadened. The isonicotinate ligands of **3** provide another IR-active label which, like the CO bands, is sensitive to the electron density at the ruthenium centers. During the course of the first oxidation the ester band experiences a blue shift of 11 cm^{-1} (Fig. 2b). The second oxidation of **2** initially generated a new species with a single CO band at 30 cm^{-1} higher energy (Fig. 3a). Even rapid electrolysis did not enable full conversion of $\mathbf{2}^+$ before decomposition occurred. This is evidenced by increasing deviations from an isosbestic point and CO band intensity loss as the electrolysis continues. Despite this, we are confident in assigning the new band to the dication $\mathbf{2}^{2+}$. Re-electrolysis after dominant conversion to $\mathbf{2}^{2+}$ gave back the starting material in approximately 55% spectroscopic yield with concomitant collapse of the new IR feature. No such problems were encountered for the $\mathbf{1}^{+/2+}$ and $\mathbf{3}^{+/2+}$ couples. Otherwise the results were rather similar, as is indicated by a blue shift of the CO band by another 30 or 34 cm^{-1} (Fig. 3b, Table 2). In addition, the isonicotinate ester band of $\mathbf{3}^{2+}$ is observed at 11 cm^{-1} higher energies than for $\mathbf{3}^+$. Of note is the sharpening of the carbonyl absorption bands of complexes **1** and **3** on the second oxidation process.

In UV–visible and NIR spectroelectrochemistry, the first oxidation of compounds **1–3** produces a pair of fairly intense absorption bands at 450–470 and 720–800 nm, attesting to their intense blue–green coloration. The higher-energy band exhibits some vibrational coupling, with estimates for peak separations in the range 1100 to 1250 cm^{-1}. As a representative example, spectra recorded during the conversions of complexes **1** and **2** to their radical cations are displayed in Fig. 4. Complexes **1** and **3** absorb intensely near 400 nm even in the neutral state. This band originates from charge-transfer absorption from the $Ru_2C_4H_4$ entity to the peripheral isonicotinate [34] or phosphine acceptor ligands (vide infra). Features in the low-energy region of the visible range at the mixed-valence monocation stage are characteristic of intervalence charge transfer [39, 40, 41, 42] (or, for the strongly coupled Class-III case, charge-resonance [43, 44]) absorption bands. Such bands formally arise from transfer of an electron from one of the redox-active moieties to the other across the bridge and are crucial for evaluating the electronic coupling between the redox-active entities.

ESR spectra of the mixed-valence monooxidized forms of complexes **1–3** were also obtained. They have a strong isotropic signal at g_{iso} of ca 2.035 in fluid solution. Spectra recorded on frozen solutions display axial or weakly rhombic splitting of the *g*-tensor. Fitting data obtained from simulations are collected in Table 2. Of special relevance is the solution spectrum of the $\mathbf{1}^+$ radical cation which exhibits resolved couplings to other ESR-active nuclei. The experimental spectrum can be simulated by invoking different couplings to two pairs of inequivalent H nuclei corresponding to the inner and outer protons of the C_4H_4 chain, four equivalent phosphorus nuclei, and two equivalent ruthenium centers (Fig. 5). The fitting data are also provided in Table 2. In all other cases the solution spectra gave considerably broadened signals without any resolved splittings.

Table 2 Spectroscopic data for complexes**1–3** in various oxidation states

	ν(CO) in cm^{-1} ($\Delta\nu_{1/2}$ in cm^{-1})	λ_{max} in cm^{-1} (ϵ_{max})	g_{iso}; g_{anis} (half width) at 110 K[a]
1	1933 (4), 1926 (4)	25850 (3240), 34480 (sh, 14500)	
1^{+}	1962 (70)	13900 (1250), 17065 (950), 21860 (3000), 25850 (3750), 34700 (16500)	2.0336 [$a(^1H_{1,3})$ = 10 G, $a(^1H_{2,4})$ = 6 G, $a(^{31}P)$ = 4.5 G, $a(^{101}Ru)$ = 4 G, $a(^{99}Ru)$ = 3.6 G]; $g_{\|}$ = 2.0452 (30 G), $g_{\perp}$ = 2.0221 (26 G)
1^{2+}	1981 (22)		
2	1906 (18)	No bands	
2^{+}	1930 (13)	12480 (3120), 23175 (4720), 29650 (4630)	2.0380; $g_{\|}$ = 2.0464 (27 G), $g_{\perp}$ = 2.0178 (20 G)
2^{2+}	1962 (13)		
3	1927 (4), 1720 (6)[b]	24690 (9000), 29326 (30000), 37313 (44000)	
3^{+}	1950 (41), 1731 (11)[b]	13100 (2900), 21260 (7500), 24900 (10500), 37600 (43000)	2.0355; $g_{\|}$ = 2.0473 (30 G), $g_{\perp}$ = 2.0196 (22 G)
3^{2+}	1984 (22), 1742 (12)[b]		

[a] g values were obtained from simulations of the experimental spectra
[b] Isonicotinate ester band

Quantum-chemical calculations

Quantum-chemical calculations by density functional theory (DFT) methods were performed on the model complexes $[\{Ru(CO)Cl(PH_3)_3\}_2(\mu\text{-}C_4H_4)]^{n+}$ ($\mathbf{2}^{\mathbf{H}\ n+}$) and $[Ru(CO)Cl\{PMe_3)_3\}_2(\mu\text{-}C_4H_4)]^{n+}$ (n = 0,1,2) ($\mathbf{2}^{\mathbf{Me}\ n+}$) to learn about the nature of the frontier orbitals and the spectroscopic and structural changes induced by successive oxidations (details are given in the "Materials and methods" section). Geometry optimization at each oxidation state started from a symmetry-broken geometry. Nevertheless the ground state structures at each oxidation state are approximately symmetrical with an inversion center passing through the midpoint of the central C–C bond of the butadienediyl ligand. The metrical data for the ground state of neutral $\mathbf{2}^{\mathbf{Me}}$ were calculated by use of the B3LYP and BP functionals and are compared with the experimental values for $[\{(PEt_3)_3(CO)ClRu\}_2(\mu\text{-}C_4H_4)]$ (**2**) in Table 3. Pertinent atom numbering is provided in Scheme 2. The agreement between experimental and calculated values is excellent and, for most bonds, inside the range of experimental standard deviations. ADF/BP calculated bond data for $\mathbf{2}^{\mathbf{Me}}$ at different oxidation states are

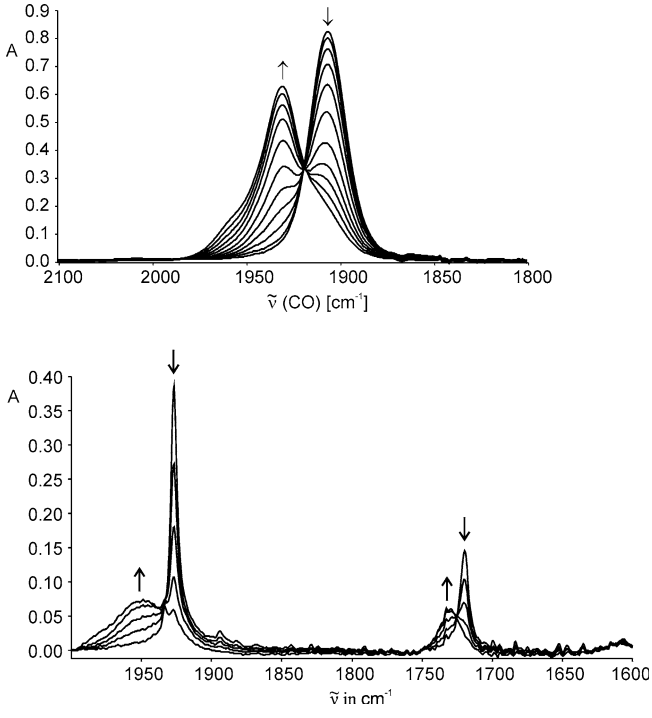

Fig. 2 IR spectroelectrochemistry: first oxidation of complexes **2** (*upper trace*) and **3** (*lower trace*) in 1,2-$C_2Cl_2H_4$/NBu_4PF_6 at 293 K

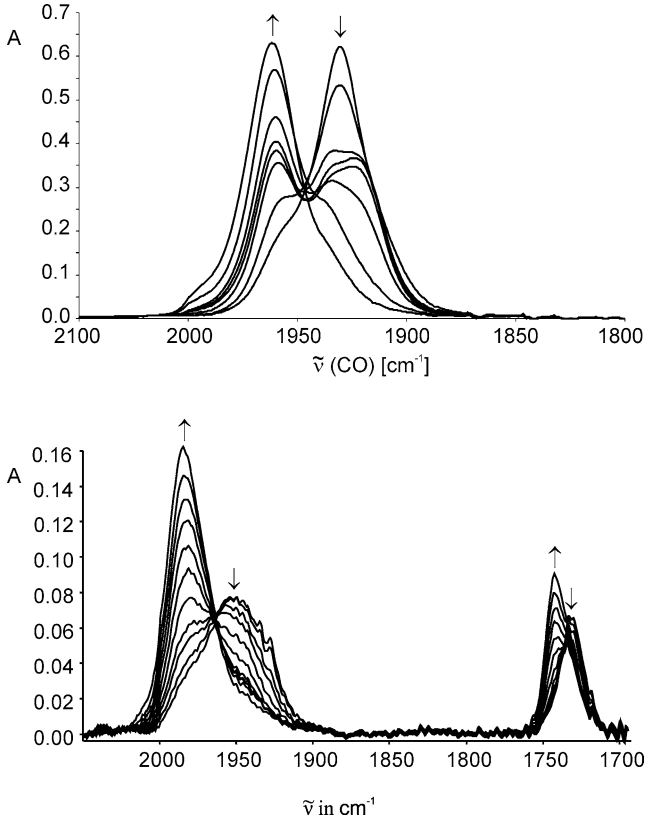

Fig. 3 IR spectroelectrochemistry: second oxidation of complexes **2** (*upper trace*) and **3** (*lower trace*) in 1,2-$C_2Cl_2H_4$/NBu_4PF_6 at 293 K

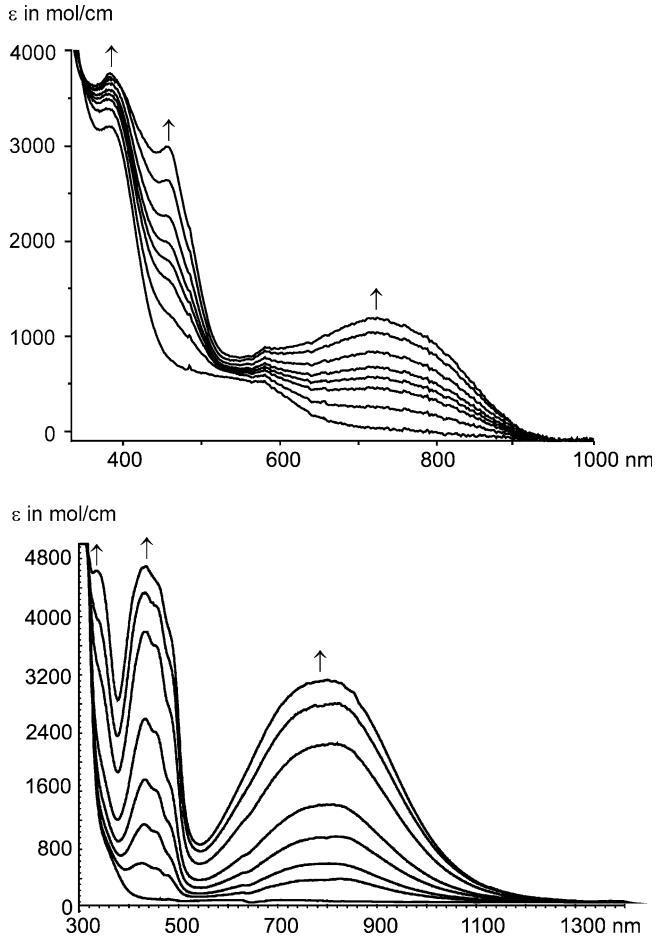

Fig. 4 UV–visible spectroelectrochemistry: first oxidation of complexes **1** (*upper traces*) and **2** (*lower traces*) in 1,2-$C_2H_4Cl_2$/NBu_4PF_6

collected in Table 4. The most important structure changes comprise lengthening of the C(1)–C(2) bond and a shortening of the Ru–C(vinyl) (Ru-C(1)) and the internal C(2)–C(2′) bonds of the C_4H_4 ligand. ADF/BP calculated compositions and energies of the frontier orbitals of $\mathbf{2^{Me}}$ show that the HOMO is delocalized over the entire $Ru_2C_4H_4$ portion of the molecule with 62% contribution from the C_4H_4 ligand and 33% contribution from the ruthenium atoms (Table 5). The issue of CO band shift on oxidation was addressed by calculating the vibrational frequencies for $[\{Ru(CO)Cl(PMe_3)_3\}_2(\mu\text{-}C_4H_4)]^{n+}$ ($\mathbf{2^{Me\ n+}}$, $n=0,1,2$) at the G03/BP86 level of theory. The symmetric and antisymmetric combinations of the Ru(CO) stretches are nearly degenerate with mean values of 1911 ($n=0$), 1935 ($n=1$), and 1964 ($n=2$) cm^{-1}. Although these values are offset by approximately 15 cm^{-1} relative to the experimental values, the presence of just one band in each oxidation state and the absolute magnitude of the overall shift upon each oxidation step give an almost perfect match with experimental results.

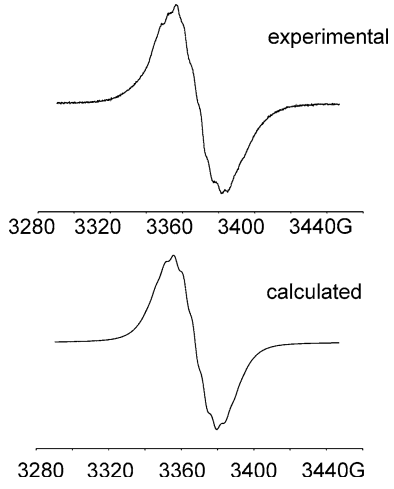

Fig. 5 Experimental and calculated ESR spectrum of electrogenerated $\mathbf{1}^+$ in fluid solution (CH_2Cl_2, 303 K)

Discussion

Arrays that consist of two redox-active moieties and a conducting bridge constitute the most basic model of a molecular wire [45, 46, 47, 48, 49]. A central issue in this respect is the ability of the bridge to provide a pathway for efficient charge and spin delocalization. Connecting the wires to the "outside world" and direct testing of their conductivity is, however, difficult to accomplish [47, 50, 51]. A simpler, more common approach is to incorporate the wire into a bridging ligand, attach redox active moieties to both ends, oxidize (or reduce) one of these, and probe for the rate at which the odd electron is transferred between the peripheral redox sites. A basic requirement for efficient "electronic communication" is good orbital overlap between the redox sites and the bridge. A differentiation of "end group",

Table 3 Comparison of selected DFT calculated bond lengths and angles with experimental values for $[\{RuCl(CO)(PMe_3)_3\}_2(\mu\text{-}CH=CHCH=CH)]$ ($\mathbf{2^{Me}}$)

	G03/B3LYP	ADF/BP	Experimental[a]
Ru–C(3)	1.821	1.820	1.834(9)
Ru–Cl	2.507	2.514	2.484(2)
Ru–C(1)	2.080	2.109	2.088(8)
Ru–P(1)	2.428	2.418	2.400(2)
Ru–P(2)	2.524	2.444	2.440(3)
Ru–P(3)	2.426	2.398	2.397(2)
C(1)–C(2)	1.366	1.357	1.34(2)
C(2)–C(2′)	1.467	1.462	1.44(1)
C(3)–O	1.186	1.180	1.13(1)
Ru–C(1)–C(2)	132.3	131.5	132.0(6)
C(1)–C(2)–C(2′)	124.9	125.3	126(1)
Cl–Ru–C(1)	89.2	89.2	88.8(2)
C(1)–Ru–C(3)	92.6	91.5	89.9(3)
C(1)–Ru–P(1)	81.8	80.4	81.0(2)
C(1)–Ru–P(2)	177.3	179.2	178.9(2)
C(1)–Ru–P(3)	83.7	81.0	81.2(2)

[a]Experimental data for $[\{RuCl(CO)(PEt_3)_3\}_2(\mu\text{-}CH=CHCH=CH]$

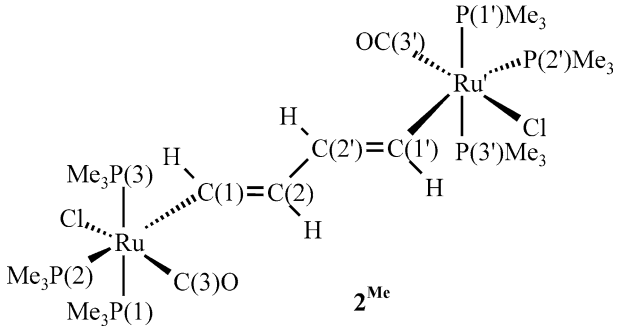

2^{Me}

Scheme 2

"bridge", and "spacer" has been made by Launay [52]. This, in essence, means that the frontier molecular orbitals must be delocalized across the entire system. As will be detailed below, butadienediyl-bridged diruthenium complexes meet this requirement in a particularly favorably manner.

Electrochemistry

Electrochemistry is frequently regarded as a first indicative probe of the extent of electron delocalization (the so-called "electronic coupling") between redox sites. The quantity of interest is the splitting between individual redox events, $\Delta E_{1/2}$. $\Delta E_{1/2}$ is easily obtained from voltammetric measurements and relates directly to the comproportionation equilibrium constant K_c (Eq. 2). K_c is a measure of the thermodynamic stability of the intermediate redox state. According to common belief, the differences between individual half-wave potentials, and thus K_c, increase with stronger redox-site interactions across the bridging ligand. Such notions have, however, been met with criticism. In fact, redox potentials, and also their differences, depend on a variety of factors other than the "electronic stabilization" of the mixed-valence state [53, 54, 55], and these other contributions may even dominate the observed potential splitting. Thus, there are several examples of intrinsically delocalized behavior despite relatively small $\Delta E_{1/2}$ values [56, 57]. Nevertheless, convincing cases have been made for the validity of such correlations. Studies by Geiger et al. have revealed a close correspondence between a spectroscopically derived charge-distribution parameter and $\Delta E_{1/2}$ values within series of closely related systems [58, 59, 60]. Likewise, Lambert et al. have shown that the electronic coupling parameter V_{AB} derived from the IVCT transitions in the near infrared correlates well with electrochemically determined $\Delta E_{1/2}$ values [61]. Ito and Kubiak have reported intriguing examples of a correlation between $\Delta E_{1/2}$ values and the rate of intramolecular electron transfer between bridged triruthenium sites [62]. Within the series of butadienediyl bridged di-iron complexes, however, only fair agreement was observed between $\Delta E_{1/2}$ and V_{AB} [14]:

$$\mathrm{Red}-\mathrm{Red}+\mathrm{Ox}-\mathrm{Ox}\leftrightarrows 2\ \mathrm{Red}-\mathrm{Ox} \quad (1)$$

$$K_c=\frac{[\mathrm{Red}-\mathrm{Ox}]^2}{[\mathrm{Red}-\mathrm{Red}][\mathrm{Ox}-\mathrm{Ox}]}=\exp\{(nF/RT)\Delta E_{1/2}\} \quad (2)$$

Keeping these caveats in mind, the large K_c values of 3.2×10^{11} and 5.3×10^{9} for $\mathbf{2}^+$ and $\mathbf{3}^+$ are within the range usually associated with mixed-valence compounds of Class-III for which no thermal barrier for intramolecular electron transfer exists. Such compounds are intrinsically delocalized even on short experimental time scales. The K_c values for the coordinatively unsaturated **1** is, however, much smaller, such that its monooxidized form may be at the borderline of Class-II and Class-III behavior. In this special situation assignment to a valence-localized or delocalized system may depend on the timescale of the experimental probe [41, 63]. We note that the butadienediyl bridged di-iron complexes [{(η^5-

Table 4 Selected ADF/BP calculated bond data for the model complex $[\{RuCl(CO)(PMe_3)_3\}_2(\mu\text{-}CH=CHCH=CH)]^{n+}$ ($\mathbf{2}^{Men+}$)

	$n=0$	$n=1$	$n=2$
Ru–C(3)	1.820	1.832	1.847
Ru–Cl	2.514	2.481	2.449
Ru–P(1)	2.418	2.437	2.489
Ru–P(2)	2.444	2.492	2.555
Ru–P(3)	2.398	2.426	2.458
Ru–C(1)	2.109	2.023	1.949
C(1)–C(2)	1.357	1.393	1.430
C(2)–C′(2)	1.462	1.418	1.384
C(3)–O	1.180	1.174	1.169
Ru–C(1)–C(2)	131.5	131.0	130.4
C(1)–C(2)–C(3)	125.3	124.3	123.5
Cl–Ru–C(1)	89.2	88.9	87.8
C(1)–Ru–C(3)	91.5	92.6	94.4
C(1)–Ru–P(1)	80.4	82.8	83.4
C(1)–Ru–P(2)	179.2	179.0	176.2
C(1)–Ru–P(3)	81.0	85.2	86.7

Table 5 Calculated ADF/BP electron energies and compositions of the frontier orbitals for the model complex $[\{RuCl(CO)(PMe_3)_3\}_2(\mu\text{-}CH=CHCH=CH)]$ (per cent contributions according to Mulliken population analysis)

MO	E in eV	Dominating character	Ru	C_4H_4	PMe_3	CO	Cl
LUMO + 1	–0.43	Ru + (PMe_3)	50(d)	0	34	8	8
LUMO	–0.45	Ru + (PMe_3)	51(d)	0	35	7	7
HOMO	–3.35	$\pi(C_4H_4)$ + Ru	33(d)	62	5	0	0
HOMO-1	–4.28	Ru + Cl	47(d)	7	8	9	29
HOMO-2	–4.30	Ru + Cl	42(d)	8	9	9	32

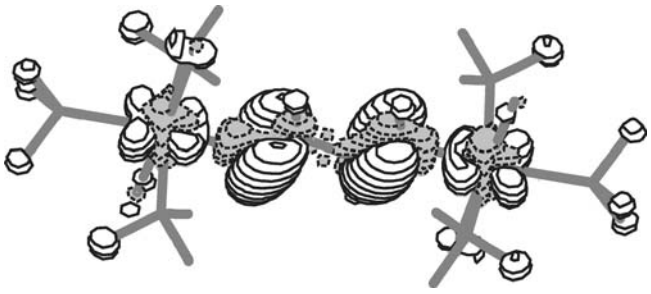

Fig. 6 Computed electron density differences for the first oxidation of the model complex $[\{RuCl(CO)(PH_3)_3\}_2(\mu\text{-}CH=CH\text{–}CH=CH)]$ ($\mathbf{2^H}$); loss of electron density is shown in *white* and an increase is shown in *grey*

$C_5R_5)LL'Fe\}_2(\mu\text{-}C_4H_4)]$ (R = H, Me, LL′ = dppm, R = H, LL′ = dppe, L = CO, L′ = PPh_3, PMe_3) and $[\{(\eta^5\text{-}C_5Me_5)(dppm)Fe\}_2(\mu\text{-}C_4H_2(OMe)_2\text{-}1,4)]$ have K_c values in the range 1.9×10^7 to 1.1×10^{12}, similar to **2** and **3**. Their mixed valence forms were assigned as Class-III species on the basis of extensive spectroscopic investigations [14].

IR spectroelectrochemistry

Because of its short inherent timescale of 10^{-12} s, IR spectroscopy is usually regarded as the most indicative probe for valence delocalization. Complexes **1**–**3** are particularly well suited for such studies. They contain a single CO moiety at each metal end group. Because vibrational coupling between the symmetric and antisymmetric stretching modes is negligible, they give rise to just one CO band in their reduced state. Owing to the synergistic nature of the metal–CO bond, the position of this band closely reflects the electron density at the metal to which the carbonyl ligand is bonded. Because the electron density at the metal diminishes on oxidation, metal-to-CO back-bonding is weakened and the CO stretch shifts to higher energy. In general, the CO shifts amount to >100 cm^{-1} for a metal centered oxidation process, making this band a particularly sensitive probe.

The monooxidized forms of complexes **1** to **3** give a single IR carbonyl band but band shape differences are still substantial, especially when compared with the reduced state. In **2**, the band widths are very similar for each oxidation state. This is clearly not so for **3** (Fig. 2b). In fact, the half width increases from 4 cm^{-1} in **3** to about 40 cm^{-1} in $\mathbf{3}^+$. One possible explanation is that the observed band constitutes an overlap of two closely spaced individual features. The other possibility is exchange broadening. In general, such a phenomenon is observed when the rate of chemical exchange competes with the timescale of the spectroscopic experiment. To be detected in IR spectroscopy, the rate of such a process must be of the order of 1×10^{11} to 1×10^{12} s^{-1}. IR exchange broadening because of intramolecular electron transfer has ample literature precedence [62, 64, 65]. Attempts to fit the experimental band to two separate Gaussian peaks with half-widths similar to that in the reduced and the fully oxidized states gave less satisfactory results than simulation involving a single broad absorption. This lets us favor the second explanation but we concede that a more definite answer must await detailed analysis of the effects of temperature and solvent on band shape. Both possible explanations place $\mathbf{3}^+$ close to the borderline of Class-II and Class-III behavior. They differ, however, with respect to its character as a valence-localized or delocalized species.

IR spectroelectrochemical investigations of the $\mathbf{1}/\mathbf{1}^+$ conversion were complicated by the low solubility of this complex. Spectroelectrochemical experiments had to be performed on a fine suspension rather than on a solution. This may also be the underlying reason for the two-band pattern observed for **1**. Upon oxidation the CO band became exceedingly broad, with a half-width $\Delta\nu_{1/2}$ of ca 70 cm^{-1}, and distinctly asymmetric. While the band envelope was best reproduced by invoking two different absorptions at 1936 and 1972 cm^{-1}, the low intensity of this band, the unfavorable signal-to-noise ratio, and the possible presence of a mixture of dissolved and undissolved species prevents us from drawing any safe conclusions from this experiment.

The fully oxidized forms of **1**–**3** display only one CO band which is further shifted to higher energy when compared with the monocations. For $\mathbf{1}^{2+}$ and $\mathbf{3}^{2+}$ the CO band is seen to sharpen again such that the half-width diminishes to 22 cm^{-1}. Comparison of the CO band energies for the neutral and the dication states is quite revealing: The overall shift amounts to ca 55 cm^{-1}, roughly half the value expected for a metal centered one-electron oxidation of a Ru complex. This points to considerable charge delocalization onto the bridging ligand. In keeping with this observation, quantum chemical studies on the $[\{RuCl(CO)(PMe_3)_3\}_2(\mu\text{-}CH=CHCH=CH)]$ ($\mathbf{2^{Me}}$) model complex gave a 62% contribution from the bridge and a 38% contribution from the two $\{Ru(CO)(PMe_3)_3Cl\}$ moieties. Computed charge density differences for the simplified $\mathbf{2^H}$ model where the PMe_3 ligands are replaced by PH_3 (Fig. 6) underscore a major contribution of the bridge and a smaller one from the metal centers. The isonicotinate ester functions of **3** provide a second IR probe for charge delocalization in the various oxidation states and the overall metal contribution to the oxidation processes. This band shifts by 11 cm^{-1} for each oxidation step. Significantly smaller shifts of just 4 cm^{-1} were observed for the analogous *meta*-divinylphenylene-bridged complexes $[\{Ru(PPh_3)_2(CO)Cl(NC_5H_4COOEt\text{-}4)\}_2(\mu\text{-}CH=CH\text{–}C_6H_4\text{–}CH=CH\text{–}1,3)]$, where the metal contribution to the HOMO was computed as only 17% [34]. In accord with a lower metal contribution, the overall CO shift is reduced to 46 cm^{-1}, compared with 57 cm^{-1} in **3**. In mononuclear $[Ru(PPh_3)_2(CO)Cl(NC_5H_4COOEt\text{-}4)(CH=CHPh)]$ the CO and COOEt band-shifts amount to 39 and 4 cm^{-1}, respectively (Maurer and Winter, unpublished results). We note, again, that the overall magnitudes of the CO shifts are

well reproduced by quantum chemistry. In the butadienediyl-bridged iron complex [{(η^5-C_5H_5)(CO)(PPh_3)Fe}$_2$(μ-C_4H_4)], the carbonyl CO band shifts by 34 and 66 cm^{-1} with respect to the neutral starting compound upon the first and second oxidation steps. The larger magnitude of these shifts may correspond to a higher contribution of the lower-lying metal based orbitals to the HOMO in these iron complexes.

ESR spectroscopy

ESR spectroscopy is the method of choice for mapping the SOMO of an odd-electron species. In our case it complements the IR technique, insofar as it provides information on *spin* as opposed to *charge* localization or delocalization across the $Ru_2C_4H_4$ array. This technique also enables differentiation between metal and ligand centered odd-electron species. Metal-based Ru(III) radicals are ESR-silent in fluid solution, because of rapid relaxation. In the frozen state they have rhombic or axial *g*-tensors with clearly detectable *g*-tensor anisotropies and distinct deviations of the average *g*-value, g_{av}, from that of the free electron, g_{el} ($g_{el} = 2.0023$). Organic radicals, on the other hand, give strong and often richly structured ESR signals in fluid solution, isotropic *g*-tensors in the frozen state, and *g*-values in the close vicinity of g_{el}. Monooxidized $\mathbf{1}^+$ to $\mathbf{3}^+$ give strong signals at *g*-values of approximately 2.035 even at room temperature and are therefore assigned as mainly organic in nature. The notable deviations from the free electron value, however, suggest substantial admixture of metal character to the singly occupied molecular frontier orbitals (SOMO). This is also reflected by a slight axial splitting of the *g*-tensor in the frozen state (Table 2).

Of note are the experimentally observed hyperfine splittings for $\mathbf{1}^+$. Spectral simulations suggest that the unpaired spin is coupled to two equivalent pairs of hydrogen atoms from the butadienediyl ligand (10.0 and 6.0 G), and to four equivalent phosphorus (4.5 G) and two identical ruthenium nuclei (4.0 and 3.6 G for ^{101}Ru and ^{99}Ru). This provides direct evidence that mixed-valence $\mathbf{1}^+$ is *intrinsically delocalized* on the timescale of the ESR experiment (10^{-9} s). All other spectra were noticeably broad with no resolved couplings. This may be because of the presence of further ligands with other ESR active nuclei (^{15}N, ^{31}P) directly bonded to the ruthenium centers. Additional couplings may broaden the spectra beyond any resolution, because of strongly overlapping resonance lines or an overall increase in line widths. Quantum chemical calculations agree well with the experimental observations. ADF/BP calculations for $\mathbf{2}^{\mathbf{Me}+}$ predict a g_{iso} value of 2.048 and rhombic splitting of the *g* tensor with $g_1 = 2.068$, $g_2 = 2.038$, and $g_3 = 2.035$, which are a good match with our experimental data.

It is again interesting to compare the ruthenium complexes to their iron counterparts. We note that the [{(η^5-C_5H_5)Fe(CO)(PPh_3)}$_2$(μ-C_4H_4)]$^+$ [11] and [{(η^5-C_5Me_5)Fe(dppm)}$_2$(μ-C_4H_2(OMe)$_2$-1,4)]$^+$ radicals [46] behave in an essentially identical manner. Couplings of 1.9, 3.3, and 7.0 or 1.9, 3.3, and 8.05 G were observed for the different diastereomers of the dicarbonyl complex and these were assigned as arising from the two inner and the two outer protons of the bridge and from the four phosphorus nuclei. Similar other derivatives gave only broadened spectra without any resolved couplings at g_{iso} values ranging from 2.024 to 2.102 [14]. Likewise, rhombic splittings of the *g*-tensors were observed in the frozen state. The larger couplings to the C_4H_4 protons and reduced couplings to the phosphorus nuclei in $\mathbf{1}^+$ to $\mathbf{3}^+$ are another indication of a lower metal contribution to the SOMO compared with the iron complexes. As the butadienediyl bridging ligand contributes strongly to the SOMO of these complexes, butadienide radical anions provide another interesting point of comparison. (The bridging ligand in complexes **1–3** is viewed as butadienediide, $C_4H_4^{2-}$. A covalent model would lead to essentially identical results, because butadiene radical cations have similar spectroscopic properties.) Parent butadienide has couplings of 7.62 and 2.79 G [66] whereas values of 7.15 and 4.92 (outer protons) and 2.40 and 1.91 G (inner protons) have been reported for the *s-trans* forms of the 1,4-di-^{t}butylbutadienide [67] and the 1,4-diphenylbutadienide [68] radical anions.

UV–visible and NIR spectroscopy

Intervalence charge-transfer bands in the low-energy part of the visible range or in the near infrared (NIR) are typical attributes of mixed-valence compounds and crucial for determining the electronic coupling term H_{AB}. H_{AB} relates to the vertical energy difference between the asymmetrically and symmetrically coupled potential energy surfaces for the two degenerate limiting electronic structures [M^+–B–M] and [M–B–M^+], where M and M^+ denote the reduced and the oxidized forms of the redox active end groups and B is the connecting bridge. For valence-localized Class-II compounds the corresponding absorption can be thought of as an isomerization between two degenerate valence isomers. It is hence referred to as intervalence charge-transfer transition (IVCT). The coupling term H_{AB} is then given by Eq. (3). Here, ν_{max} and ϵ_{max} denote the energy and extinction coefficient at the band maximum, $\Delta\nu_{1/2}$ its width at half height, and r_{MM} the charge-transfer distance, that is the spatial separation between the centroids of the reduced donor and oxidized acceptor sites. In intrinsically delocalized Class-III systems this band has rather the character of an electronic transition between strongly delocalized molecular orbitals. It has thus been termed a charge resonance band [43, 44]. In this case the coupling term H_{AB} is simply half the energy at the band maximum (Eq. 4):

$$H_{AB} = 0.0206 \cdot \frac{\left(\nu_{max}\varepsilon_{max}\Delta\nu_{1/2}\right)^{1/2}}{r_{AB}} \quad (3)$$

$$H_{AB} = \nu_{max}/2 \quad (4)$$

$$\Delta\nu_{1/2} = (2310 \cdot \nu_{max})^{1/2} \quad (5)$$

Substantial difficulty arises when defining the r_{AB} term. Taking r_{AB} as the spatial separation between the metal atoms in a bridged dimetal complex is justified for weakly coupled systems with small M–bridge–M$^+$ interactions and frontier orbitals that are largely localized at the metal sites. For Class-III systems with extensively delocalized frontier orbitals this assumption is, however, no longer valid. Convincing cases have been made that H_{AB} values extracted from charge-resonance bands by applying the Hush formula (Eq. 3) underestimate the strength of the coupling by a factor of 2 to 3 when the spatial distances between the nominal redox sites are employed [14, 41, 61]. This is almost certainly true of the butadienediyl bridged complexes described herein, where the bridge dominates the SOMO orbital in the mixed-valence state.

The monocations $\mathbf{1}^+$ to $\mathbf{3}^+$ afford fairly intense ($\epsilon \approx 3000$) absorption bands with maxima at 12500 to 13900 cm^{-1} (800 to 720 nm). The bands are distinctly asymmetric and of non-Gaussian shape. Deconvolution required three overlapping, closely spaced sub-bands. Individual band widths range from 1500 to 3300 cm^{-1} which is considerably lower than those predicted from Hush theory for Class-II systems. Applying Eq. (5), which has been derived by Hush for moderately coupled Class-II systems, gives theoretical values of 5370–5670 cm^{-1} [39]. Lower band widths are usually taken as evidence of a Class-III system. Results from other spectroscopic techniques, including IR and ESR spectroscopy, also agree with a valence-delocalized (or nearly delocalized) situation. H_{AB} can then be calculated from Eq. (4), and this gives values of 0.86 ($\mathbf{1}^+$), 0.77 ($\mathbf{2}^+$), and 0.81 ($\mathbf{3}^+$) eV. Much smaller values, 0.15 ($\mathbf{1}^+$), 0.25 ($\mathbf{2}^+$), and 0.24 ($\mathbf{3}^+$) eV, are obtained by use of the Hush formula (Eq. 3). In this calculation, the average half-width for the low and high-energy side of the IVCT (or charge-resonance) band are considered for evaluation of $\Delta\nu_{1/2}$, and r_{AB} is set as 3.772 Å, which is the calculated distance between the ruthenium-bonded carbon atoms in $\mathbf{2}^{Me+}$. We prefer this definition of r_{AB} because the outer carbon atoms are associated with the highest orbital coefficients in the HOMO.

Sponsler has suggested that the $\{M\}_2C_4H_4$ entity of butadienediyl-bridged dimetal complexes is best regarded as an extended π system to which the metal entities efficiently contribute. According to his proposal the charge-resonance absorption of $\mathbf{1}^+$, $\mathbf{2}^+$ and $\mathbf{3}^+$ would involve excitation from the symmetrical combination of the d_π orbitals to the SOMO level (S1 → A2 in Fig. 7) [14]. The latter orbital is antibonding between the metal d_π orbitals and the π_2 orbital of the butadienediyl bridge, whereas the S1 orbital is mainly localized at the metal centers, because of nonbonding interaction with the π_2 orbital of the bridging ligand. Subbands may arise from d → π* transitions from other non-bonding metal-based d orbitals that are close in energy. Calculations on $\mathbf{2}^{Me+}$ are, however, required to clarify the exact nature of this transition.

Oxidation of **1**–**3** to their monocations also generates new absorptions at higher energies (430–470 nm). For $\mathbf{1}^+$ and $\mathbf{2}^+$ these bands display vibrational progressions with spacings of ca 1310 to 1100 cm^{-1}, whereas such sub-bands were not resolved for $\mathbf{3}^+$. Such behavior is typical of π → π transitions. We therefore assign these bands to transitions from the bonding to the antibonding combination of the Ru-d_π and the butadienediyl π_2 orbital (A1 → A2). In this respect we note that the radical anion and cation of *all-trans* 1,4-diphenylbutadiene also have structured absorption at 560 or 546 nm [69]. Irradiation into this band results, inter alia, in the resonance enhancement of Raman bands at 1215 and 1176 or 1250 and 1298 cm^{-1}, respectively [70]. These bands have been ascribed to polyenic CH bend and CC stretch [70, 71].

Absorption at still higher energy, at 386 and 402 nm in $\mathbf{1}^+$ and $\mathbf{3}^+$, respectively, is also present in the reduced state and, apart from some intensity loss, remain

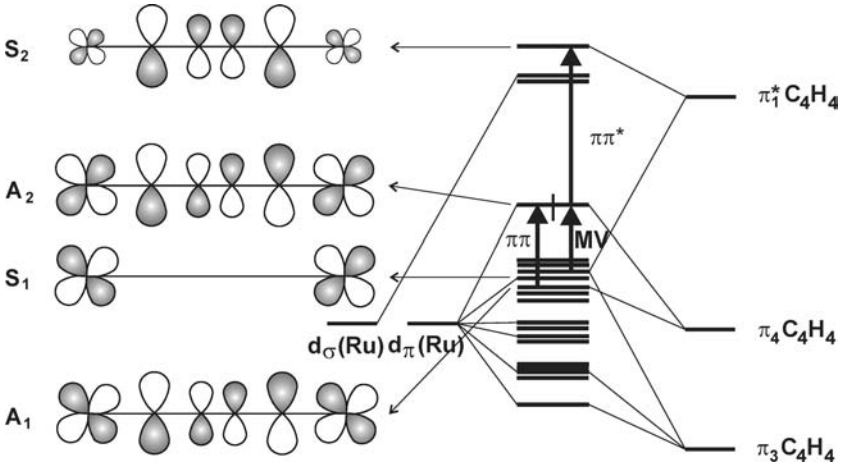

Fig. 7 Energies and schematic representations of the orbitals involved in the optical transitions

nearly unchanged on oxidation. With reference to our work on the divinylphenylene bridged complex $[\{Ru(PPh_3)_2(CO)Cl(NC_5H_4COOEt\text{-}4)\}_2(\mu\text{-}HC=CH\text{-}C_6H_4\text{-}CH=CH\text{-}1,3)]$ [34], we assign this band as a charge-transfer transition from the HOMO to the pyridine acceptor-based LUMO (**3**) or a higher lying metal phosphine-based orbital in **1**. In **2** this band is apparently shifted into the UV region owing to the increased electron density at the ruthenium site. Stronger absorptions in the UV are probably due to $\pi \rightarrow \pi^*$-type transitions involving the A2 and S2 levels.

Structural changes accompanying oxidation

Structural information about butadienediyl bridged dimetal complexes is available for $[\{Ru(PEt_3)_3(CO)Cl\}_2(\mu\text{-}C_4H_4)]$ (**2**) [16] and the di-iron complexes $[\{(\eta^5\text{-}C_5Me_5)Fe(dppe)\}_2(\mu\text{-}C_4H_4)]$ [14], and $[\{(\eta^5\text{-}C_5H_5)Fe(dppm)\}_2(\mu\text{-}C_4H_4)]^{2+}$ [12]. Because no oxidized form of a diruthenium complex has yet been characterized by this technique, we rely on the results of quantum chemical calculations when discussing the structural effects of the successive one-electron oxidations. Pertinent data for the ADF-optimized structures of the PMe_3 model complex are given in Table 4. Comparison of the data shows the intuitive result of a lengthening of the Ru–PMe_3 and Ru–C(CO) π-acceptor and shortening of the Ru–Cl π-donor bonds for each oxidation step. Of central interest are the effects on the bonding within the $Ru_2C_4H_4$ entity. Here we observe continuous shortening of the Ru–vinyl and internal C–C bonds and a lengthening of the former C=C double bonds. C–C bond lengths within the butadienediyl bridge are nearly identical at the monocation stage. Further oxidation to the dication causes inversion of the initial short–long–short to a long–short–long bond sequence within this ligand. The dication is thus best described as a 2-buten-1,3-diylidene structure with an unsaturated bis(carbene) bridging ligand (resonance form I, Scheme 3). This resonance form also agrees with the singlet ground state calculated for the $\mathbf{2H^{Me\,2+}}$ model and the diamagnetism of the related $[\{(\eta^5\text{-}C_5H_5)Fe(dppm)\}_2(\mu\text{-}C_4H_4)]^{2+}$ [12]. We note here that the X-ray structure of the latter dication and the isoelectronic neutral $[\{(\eta^5\text{-}C_5H_5)Mn(CO)_2\}_2(\mu\text{-}C_4H_2(OEt)_2\text{-}1,4]$ [72] exhibit the same long–short–long C–C bond pattern with values of 1.418(14)/1.366(20)/1.418(14) Å or 1.471(4)/1.323(4)/1.472(4) Å, respectively. Experimental C–C bond lengths for the di-iron complex agree with our calculated values within experimental error.

Conclusions

The studies presented herein support extensive electron delocalization in butadienediyl-bridged diruthenium complexes. Because of strong mixing between ruthenium and ligand-based orbitals in the HOMO these complexes can be thought of as extended π systems, and this renders meaningless any designation of the redox events as metal or ligand-centered processes. Carbonyl band shifts in the IR spectrum on successive oxidations emphasize this notion—oxidation to the dications results in an overall band shift of ca 55 cm^{-1}, about half the value expected for metal-centered oxidation of a mononuclear complex. The mixed-valent radical cations $[\{Ru(PEt_3)_3(CO)Cl\}_2(\mu\text{-}C_4H_4)]^+$ ($\mathbf{2^+}$) and $[\{Ru(PPh_3)_2(CO)Cl(NC_5H_4COOEt\text{-}4)\}_2(\mu\text{-}C_4H_4)]^+$ ($\mathbf{3^+}$) are either intrinsically delocalized Class-III species or nearly so. The situation is less clear for $[\{Ru(PPh_3)_2(CO)Cl\}_2(\mu\text{-}C_4H_4)]^+$ ($\mathbf{1^+}$). Even this last species is, however, delocalized on the slower ESR timescale, as is inferred from the hyperfine coupling pattern in fluid solution. Electronic couplings as measured from the splitting of the individual redox potentials seem to correlate with the IR spectroscopic properties of the cations. We also note that the strength of the electronic coupling (and, by inference, the intramolecular electron transfer rate) also depends on the ancillary ligands. The availability of a free coordination site in **1** provides us with an opportunity to control the d orbital energies, the metal contributions to the HOMO orbital, and, possibly, the extent of delocalization in the mixed-valent state. Work along these lines is currently being pursued in our laboratories.

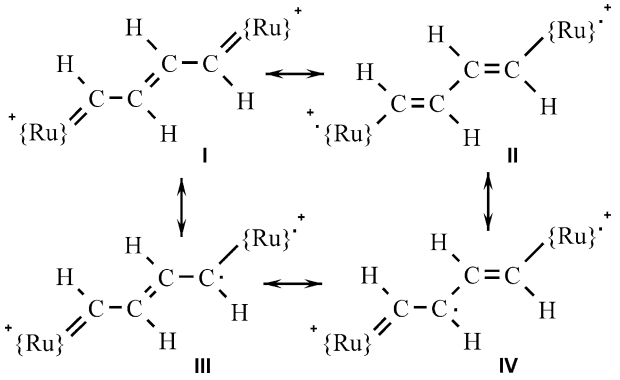

Scheme 3

Acknowledgements We gratefully acknowledge financial support of this work by the Deutsche Forschungsgemeinschaft (R.F.W., grant Wi 7/1) and by the Grant Agency of Academy of Sciences of the Czech Republic (S.Z., grant 1ET400400413).

References

1. Creutz C, Taube H (1969) J Am Chem Soc 91:3988
2. Coat F, Guillevic M-A, Toupet L, Paul F, Lapinte C (1997) Organometallics 16:5988
3. Guillemot M, Toupet L, Lapinte C (1998) Organometallics 17:1928
4. Coat F, Guillemot M, Paul F, Lapinte C (1999) J Organomet Chem 578:76
5. Fernández FJ, Blacque O, Alfonso M, Berke H (2001) Chem Commun 1266

6. Bruce MI, Low PJ, Costuas K, Halet J-F, Best SP, Heath GA (2000) J Am Chem Soc 122:1949
7. Bruce MI, Ellis BG, Low PJ, Skelton BW, White AH (2003) Organometallics 22:3184
8. Brady M, Weng W, Zhou Y, Seyler JW, Amoroso AJ, Arif AM, Böhme M, Frenking G, Gladysz JA (1997) J Am Chem Soc 119:775
9. Meyer WE, Amoroso AJ, Horn CR, Jaeger M, Gladysz JA (2001) Organometallics 20:1115
10. Robin MB, Day P (1967) Adv Inorg Chem Radiochem 10:247
11. Etzenhouser B, Cavanough MDB, Spurgeon HN, Sponsler MB (1994) J Am Chem Soc 116:2221
12. Etzenhouser BA, Chen Q, Sponsler MB (1994) Organometallics 13:4176
13. Sponsler MB (1995) Organometallics 14:1920
14. Chung M-C, Gu X, Etzenhouser BA, Spuches AM, Rye PT, Seetharaman SK, Rose DJ, Zubieta J, Sponsler MB (2003) Organometallics 22:3485
15. Guillaume V, Mahias V, Mari A, Lapinte C (2000) Organometallics 19:1422
16. Xia HP, Yeung RCY, Jia G (1998) Organometallics 17:4762
17. Ahmad N, Levison JJ, Robinson SD, Uttley MF, Wonchoba ER, Parshall GW (1974) Inorg Synth 15:45
18. Georgieff KK, Richard Y (1958) Can J Chem 36:1280
19. Krejcik M, Danek M, Hartl F (1991) J Electroanal Chem 317:179
20. Fonseca Guerra C, Snyders JG, te Velde G, Baerends EJ (1998) Theor Chim Acta 99:391
21. van Gisbergen SJA, Snijders JG, Baerends EJ (1999) Comput Phys Commun 118:119
22. Frisch MJ, Trucks GW, Schlegel HB, Scuseria GE, Robb MA, Cheeseman JR, Montgomery JA, Vreven T, Kudin KN, Burant JC, Millam JM, Iyengar SS, Tomasi J, Barone V, Mennucci B, Cossi M, Scalmani G, Rega N, Petersson GA, Nakatsuji H, Hada M, Ehara M, Toyota K, Fukuda R, Hasegawa J, Ishida M, Nakajima T, Honda Y, Kitao O, Nakai H, Klene M, Li X, Knox JE, Hratchian HP, Cross JB, Adamo C, Jaramillo J, Gomperts R, Stratmann RE, Yazyev O, Austin AJ, Cammi R, Pomelli C, Ochterski JW, Ayala PY, Morokuma K, Voth GA, Salvador P, Dannenberg JJ, Zakrzewski VG, Dapprich S, Daniels AD, Strain MC, Farkas O, Malick DK, Rabuck AD, Raghavachari K, Foresman JB, Ortiz JV, Cui Q, Baboul AG, Clifford S, Cioslowski J, Stefanov BB, Liu G, Liashenko A, Piskorz P, Komaromi I, Martin RL, Fox DJ, Keith T, Al-Laham MA, Peng CY, Nanayakkara A, Challacombe M, Gill PMW, Johnson B, Chen W, Wong MW, Gonzalez C, Pople JA (2003) Gaussian 03, Revision B2. Gaussian, Pittsburg, PA
23. Becke AD (1988) Phys Rev A 38:3098
24. Perdew JP (1986) Phys Rev A 33:8822
25. van Lenthe E, van der Avoird A, Wormer PES (1997) J Chem Phys 107:2488
26. van Lenthe E, van der Avoird A, Wormer PES (1998) J Chem Phys 108:4783
27. Andrae D, Haeussermann U, Dolg M, Stoll H, Preuss H (1990) Theor Chim Acta 77:123
28. Hariharan PH, Pople JA (1973) Theor Chim Acta 28:213
29. Stephens PJ, Devlin FJ, Cabalowski CF, Frisch MJ (1994) J Phys Chem 98:11623
30. Torres MR, Vegas A, Santos A (1986) J Organomet Chem 309:169
31. Torres MR, Santos A, Ros J, Solans X (1987) Organometallics 6:1091
32. Werner H, Esteruelas MA, Otto H (1986) Organometallics 5:2295
33. Santos A, López J, Montoya J, Noheda P, Romero A, Echavarren AM (1994) Organometallics 13:3605
34. Maurer J, Winter RF, Sarkar B, Fiedler J, Záliš S (2004) Chem Commun 1900
35. Buil ML, Esteruelas MA (1999) Organometallics 1999:1798
36. Liu SH, Chen Y, Wan KL, Wen TB, Zhou Z, Lo MF, Williams ID, Jia G (2002) Organometallics 21:4984
37. Liu SH, Xia H, Wen TB, Zhou Z, Jia G (2003) Organometallics 22:737
38. McCreery R (1986) Spectroelectrochemistry. In: Rossiter BW, Hamilton JF (eds) Electrochemical methods, vol II. Wiley, New York, p 591
39. Hush NS (1967) Prog Inorg Chem 8:391
40. Wong KY, Schatz PN (1981) Prog Inorg Chem 28:369
41. Nelsen SF (2000) Chem Eur J 6:581
42. Brunschwig B, Creutz C, Sutin N (2002) Chem Soc Rev 31:168
43. Badger B, Brocklehurst B (1970) Trans Faraday Soc 66:2939
44. Szeghalmi AV, Erdmann M, Engel V, Schmitt M, Amthor S, Kriegisch V, Nöll G, Stahl R, Lambert C, Leusser D, Stalke D, Zabel M, Popp J (2004) J Am Chem Soc 126:7834
45. Aviram A, Ratner MA (1974) Chem Phys Lett 29:277
46. Paul F, Lapinte C (1998) Coord Chem Rev 178/180:431
47. Tour JM (2000) Acc Chem Res 33:791
48. Launay J-P (2001) Chem Soc Rev 30:386
49. Robertson N, McGowan CA (2003) Chem Soc Rev 32:96
50. Weber HB, Reichert J, Weigend F, Ochs R, Beckmann D, Mayor M, Ahlrichs R, von Löhneysen H (2002) Chem Phys 281:113
51. Xu B, Tao NJ (2003) Science 301:1221
52. Launay J-P (2001) Chem Soc Rev 30:386
53. Sutton JE, Taube H (1981) Inorg Chem 20:3125
54. Launay J-P, Coudret C (2001) In: De Silva AP, Balzani V (eds) Electron transfer in chemistry, vol 5. VCH, Weinheim, chap 1
55. Barrière F, Camire N, Geiger WE, Mueller-Westerhoff UT, Sanders R (2002) J Am Chem Soc 124:7262
56. Glöckle M, Kaim W, Fiedler J (1998) Organometallics 17:4923
57. Risko C, Barlow S, Coropceanu V, Halik M, Brédas J-L, Marder SR (2003) Chem Commun 194
58. Stoll ME, Lovelace SR, Geiger WE, Schimanke H, Hyla-Kryspin I, Gleiter R (1999) J Am Chem Soc 121:9343
59. Atwood CG, Geiger WE (2000) J Am Chem Soc 122:5477
60. Bühl M, Thiel W (2004) Inorg Chem 43:6377
61. Lambert C, Nöll G (1999) J Am Chem Soc 121:8434
62. Ito T, Hamaguchi T, Nagino H, Yamaguchi T, Kido H, Zavarine IS, Richmond T, Washington J, Kubiak CP (1999) J Am Chem Soc 121:4625
63. Atwood CG, Geiger WE, Rheingold AL (1993) J Am Chem Soc 115:5310
64. Yamaguchi T, Imai N, Ito T, Kubiak CP (2000) Bull Chem Soc Jpn 73:1205
65. Londergan CH, Salsman JC, Ronco SR, Dolkas LM, Kubiak CP (2002) J Am Chem Soc 124:6236
66. Levy DH, Myers RJ (1964) J Chem Phys 41:1062
67. Gerson F, Hopf H, Merstetter P, Mlynek C, Fischer D (1988) J Am Chem Soc 120:4815
68. Schenk R, Huber W, Schade P, Müllen K (1988) Chem Ber 121:2201
69. Ayoama T, Yamamoto Y, Hayashi K (1989) J Chem Soc, Faraday Trans I 85:3353
70. Dudev T, Kamisuki T, Akamatsu N, Hirose C (1991) J Phys Chem 95:4999
71. Kamisuki T, Hirose C (1998) J Mol Struct 453:107
72. Rabier A, Lugan N, Geoffroy GL (1994) Organometallics 13:4676